Hindawi Publishing Corporation
Journal of Nanomaterials
Volume 2016, Article ID 8393648, 10 pages
http://dx.doi.org/10.1155/2016/8393648

Research Article

Preparation of TiO_2/Activated Carbon Composites for Photocatalytic Degradation of RhB under UV Light Irradiation

Baolin Xing,[1,2] Changliang Shi,[1] Chuanxiang Zhang,[1] Guiyun Yi,[1,2] Lunjian Chen,[1] Hui Guo,[1] Guangxu Huang,[1] and Jianliang Cao[1]

[1]*School of Materials Science and Engineering, Henan Polytechnic University, Jiaozuo 454003, China*
[2]*Department of Chemical Engineering, University of Newcastle, Callaghan, NSW 2308, Australia*

Correspondence should be addressed to Guiyun Yi; guiyunyi@163.com and Jianliang Cao; caojianliang@hpu.edu.cn

Received 30 October 2015; Revised 23 December 2015; Accepted 26 January 2016

Academic Editor: Cunming Liu

Photocatalysts comprising nanosized TiO_2 particles on activated carbon (AC) were prepared by a sol-gel method. The TiO_2/AC composites were characterized by X-ray diffraction (XRD), thermogravimetric (TG) analysis, nitrogen adsorption, scanning electron microscope (SEM), transmission electron microscope (TEM), and energy dispersive X-ray (EDX). Their photocatalytic activities were studied through the degradation of Rhodamine B (RhB) in photocatalytic reactor at room temperature under ultraviolet (UV) light irradiation and the effect of loading cycles of TiO_2 on the structural properties and photocatalytic activity of TiO_2/AC composites was also investigated. The results indicate that the anatase TiO_2 particles with a crystal size of 10–20 nm can be deposited homogeneously on the AC surface under calcination at 500°C. The loading cycle plays an important role in controlling the loading amount of TiO_2 and morphological structure and photocatalytic activity of TiO_2/AC composites. The porosity parameters of these composite photocatalysts such as specific surface area and total pore volume decrease whereas the loading amount of TiO_2 increases. The TiO_2/AC composite synthesized at 2 loading cycles exhibits a high photocatalytic activity in terms of the loading amount of TiO_2 and as high as 93.2% removal rate for RhB from the 400 mL solution at initial concentration of 2×10^{-5} mol/L under UV light irradiation.

1. Introduction

Dyes, generated by various manufacture industries such as dyestuffs, textile, paper, food, cosmetics, leather, and plastics, are the most common contaminants in wastewater [1–3]. These dyes appearing in wastewater, even at very low concentrations, are highly noticeable and can potentially hurt human health. However, presently, there is still no unique treatment that is capable of effectively eliminating all types of dyes in wastewater because of their complex structure and stable chemical property and diversity [4, 5]. Therefore, it is highly important to find out an effective method for treating industrial effluent such as dyes.

Currently, a number of techniques and processes including physical, chemical, and biological methods have been studied to treat the dyes from wastewater [6–10]. For instance, adsorption and photocatalysis have been considered as effective approaches for dye removal. The adsorption is a nondestructive process, by which the contaminants can be transferred from wastewater to adsorbent such as activated carbon (AC). However, the adsorption efficiency of the adsorbents after regeneration is greatly reduced [11, 12]. In comparison, the photocatalysis is a promising advanced oxidation process, which usually uses heterogeneous titanium dioxide (TiO_2) as a photocatalyst to degrade the contaminants by the decomposition and oxidation processes on its surface [13–15]. However, there are some disadvantages of TiO_2 used in advanced oxidation process as TiO_2 powder is easy to agglomerate, with poor adsorption capacity, and is difficult to be separated and recycled from the solution [5, 16, 17]. For the purpose of overcoming the drawbacks of these two approaches, the combination of adsorption and photocatalytic processes was previously proved to be a very promising technology for the treatment of wastewater. For instance, some different types of composites including ordered mesoporous TiO_2/silica nanocomposites [18], TiO_2/

alumina composites [19], TiO_2/diatomite composites [20], TiO_2/zeolite nanocomposites [21], TiO_2/clay composites [22], TiO_2/bentonite composites [23], TiO_2/reduced graphene oxide nanocomposites (TiO_2/RGO) [24], TiO_2/activated carbon fiber (TiO_2/ACF) [25], TiO_2/carbon nanotube (TiO_2/CNT) [26], TiO_2/graphene (TiO_2/GR) [27], and TiO_2/activated carbon (TiO_2/AC) [5] have been extensively studied. As AC possesses a large specific surface area, high adsorption capacity, and suitable pore structure [8, 13, 28], TiO_2/AC composites are receiving considerable attention for the degradation of dye-containing wastewater. Wang et al. [29] successfully prepared TiO_2/AC composites by dip-hydrothermal method using peroxotitanate as the TiO_2 precursor for degradation of methyl orange. Slimen et al. [28] investigated the TiO_2/AC composites which were directly obtained by sol-gel method for the degradation of methylene blue in an aqueous solution. Jamil et al. [30] synthesized photocatalyst by AC impregnated with TiO_2 for the removal of methyl orange from water, and the synergistic effects of adsorption and photocatalytic activity in TiO_2/AC for the degradation of the methyl orange have been found. Eliyas et al. [17] prepared a TiO_2/AC composite by an original method combining impregnation and physicochemical pyrolysis, and the photocatalytic decomposition of an azo dye pollutant under visible light illumination and ultraviolet (UV) light irradiation was studied. Zhang et al. and He et al. [6, 31] investigated the degradation of methyl orange and Rhodamine B (RhB) by microwave-induced photocatalytic technology using TiO_2/AC composites.

Among the reported processes for the treatment of the dye-containing wastewater, it has been shown that all kinds of TiO_2/AC composites are able to exhibit enhanced photocatalytic performance and increased removal efficiency compared to pure TiO_2. However, one of critical problems still hindering further large scale application of the TiO_2/AC composites in wastewater treatment is the lack of reproducibility due to the variation in the preparation and treatment processes [32]. Hence, it is necessary to develop a simple and low-cost method to prepare TiO_2/AC composites. Due to the simple synthesis routes and properly controlled morphology of TiO_2 on AC, the sol-gel technique is the most commonly used chemical method for the preparation of TiO_2/AC [15]. However, to the best of our knowledge, many researches focused on the photocatalytic activity, degradation mechanism and kinetics, the synergistic effects, and the role of the chemical and textural properties of AC during photocatalytic degradation of organic contaminants in wastewater [13, 17, 33], but there is little information available concerning the effect of loading cycle on the structural properties and photocatalytic activity of the final TiO_2/AC composites.

In this work, the coal-based AC (prepared by KOH activation) was adopted as a support to synthesize the TiO_2/AC composites under different loading cycles by sol-gel method. The adsorption properties and photocatalytic activity were investigated in aqueous solution using Rhodamine B (RhB) dye as a model contaminant for the photodegradation experiments. Such molecule is usually present in the wastewater from several industries.

2. Experimental

2.1. Materials. Activated carbon (AC) was prepared from lignite by potassium hydroxide (KOH) activation as described in our previous work [34]. In this procedure, activation was performed at 800°C for 2 h at 2 : 1 weight ratio of KOH to lignite. The specific surface area and total pore volume of the as-obtained AC are 1576 m^2/g and 0.967 cm^3/g, while its ash content is only 0.3%. Tetrabutyl titanate ($Ti(OC_4H_9)_4$), ethanol, acetic acid, nitric acid, potassium hydroxide, and RhB were of analytical grade and used without further purification. All the reagents were supplied by Tianjin Kemiou Chemical Reagent Co., Ltd., China.

2.2. Preparation of TiO_2/AC Composites. TiO_2/AC composites were synthesized using $Ti(OC_4H_9)_4$ as a precursor by sol-gel route as follows: First, solution A was prepared by diluting 10 mL $Ti(OC_4H_9)_4$ with 34 mL anhydrous ethanol and 2.5 mL acetic acid. Second, solution B was prepared by mixing 17 mL anhydrous ethanol with 3 mL deionized water and the pH value of the solution was adjusted to 2-3 by slowly adding dilute nitric acid. Third, solution B was transferred into solution A drop by drop with vigorous stirring to produce the TiO_2 sol. The sol was mixed with the as-prepared AC under continuous magnetic stirring and the mixture was aged for 20 h in dark area at ambient temperature to form the sol-coated AC. The mixture was washed sequently with ethanol and deionized water to remove untreated product and the solid was collected by centrifugation during each wash. The aging and washing procedures were repeated 3 times; each loading cycle of the final sol-coated AC was dried for 4 h at 110°C and then was calcined at 500°C for 3 h in a nitrogen atmosphere with a heating rate of 10°C/min. Simultaneously, the aged gel was also calcined at 500°C for 3 h to synthesize the pure nanosized TiO_2 for comparison. The TiO_2/AC composites were synthesized at 1, 2, and 3 loading cycles, which were named TiO_2/AC-1, TiO_2/AC-2, and TiO_2/AC-3, respectively.

2.3. Characterization of TiO_2/AC Composites. X-ray diffraction (XRD) experiments of the samples were performed on a Bruker-AXS D8 advance diffractometer with Cu Kα radiation, and the crystal size was calculated by X-ray line broadening analysis using Scherrer formula [13, 28, 35]: $D = 0.89\lambda/\beta\cos\theta$, where D is the crystalline size in nm, λ (0.15418 nm) is the wavelength of X-ray radiation, and β is the line width at half maximum height for the anatase (101) peak ($2\theta = 25.3^\circ$) in radians. The morphology and elemental analysis of the TiO_2/AC composites were examined by a scanning electron microscope (JSM-6390LV, Japan), a transmission electron microscope (JEM-2100, Japan), and an energy dispersive X-ray spectroscopy detector (JSM-5200, Japan). The TiO_2/AC composites were analyzed by a thermogravimetric (TG) analyzer (STA409 PC, Germany) in a range of 20–800°C with a heating rate of 10°C/min in an air flow, and the TiO_2 loading amount was calculated by ash weight (minus the ash weight of AC). Brunauer-Emmett-Teller (BET) specific surface area

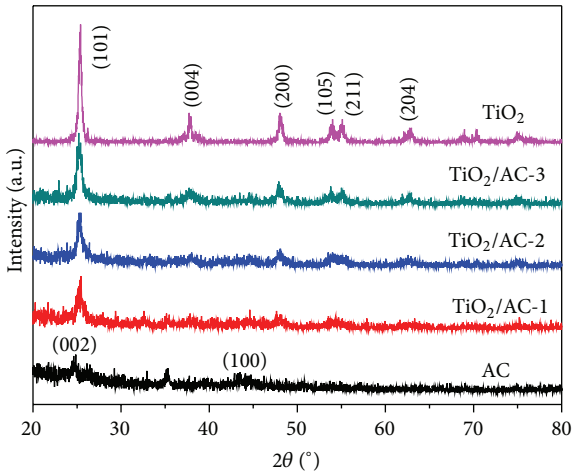

FIGURE 1: XRD patterns of AC and pure TiO_2 and TiO_2/AC composites.

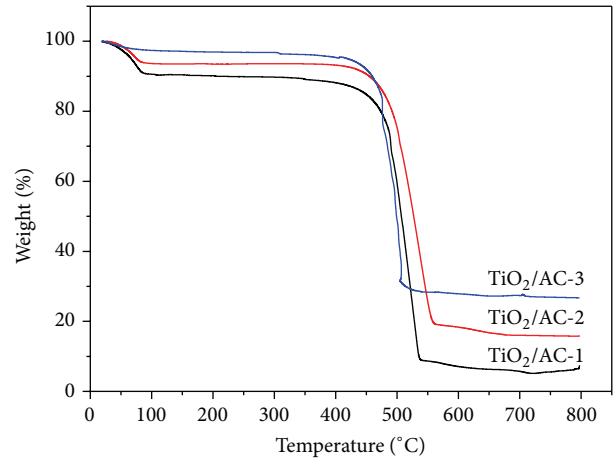

FIGURE 2: TG curves of TiO_2/AC composites.

of the AC and photocatalyst samples was measured from the nitrogen adsorption-desorption isotherms at 77 K on an automatic adsorption instrument (Quantachrome, Autosorb-iQ-MP, USA), and the pore size distribution was determined by a density functional theory (DFT) model. All samples were degassed under vacuum at 200°C for 12 h prior to the nitrogen adsorption analysis.

2.4. Photocatalytic Degradation Experiments. The photocatalytic activity experiment of the TiO_2/AC composites was studied by the degradation of RhB under UV light irradiation in a photocatalytic reactor at room temperature. The light source was from 450 W high pressure mercury lamp (Foshan Electrical and Lighting Co., Ltd.). In each experiment, 0.02 g photocatalyst was added into 400 mL of 2×10^{-5} mol/L RhB solution under magnetic stirring and maintained in the dark for 90 min in order to allow for adsorption equilibrium, and then the suspension was irradiated under UV light. After that, about 10 mL of the suspension sample was collected at 10 min intervals during the irradiation period, which was centrifuged to remove the photocatalyst. The remaining RhB in the solution was measured at 554 nm using a spectrophotometer (TU-1810, Beijing Purkinje General Instrument Co., Ltd.). The absorbance measured was then converted to concentration, and the removal rate of RhB (R%) was calculated according to the following equation, $R\% = 100(C_0 - C)/C_0$, where C_0 and C are the concentrations of RhB before and after adsorption-degradation process, respectively. The total removal rate of RhB obtained by TiO_2/AC composites contributes to the adsorptive and photocatalytic processes.

3. Results and Discussion

3.1. Crystalline Phase Characterization. The XRD patterns of AC, pure TiO_2, and TiO_2/AC composites are shown in Figure 1. As can be seen, the XRD of AC shows two weak broad peaks at about 24.6° and 43.9°, corresponding to reflection in the (002) plane and the (100) plane of aromatic layers in carbon [36], which indicates a predominantly amorphous structure present in the AC substrate, whereas the XRD pattern of pure TiO_2 shows six main diffraction peaks at about 25.3°, 37.8°, 48.0°, 53.8°, 55.1°, and 62.8°, which can be, respectively, indexed as (101), (004), (200), (105), (211), and (204) planes of an anatase TiO_2 [14, 32, 37]. It suggests that the anatase TiO_2 is predominantly formed in the pure nanosized TiO_2 when the gel was calcined at 500°C. The result is in good agreement with Xue et al.'s research [13]. For the TiO_2/AC composites, it is obvious that the diffraction peak intensity improves with increasing the loading cycle. When the AC is loaded by TiO_2 1 time, the XRD pattern of TiO_2/AC-1 presents only one apparent diffraction peak at about 25.3°, whereas the six diffraction peaks mentioned above are observed obviously in the XRD pattern for TiO_2/AC-3 when the AC is loaded by TiO_2 3 times, which indicates that more TiO_2 can be loaded on the substrate AC surface with multiloading. The results demonstrate that the loading amount of TiO_2 in the composite photocatalyst is strongly affected by the loading cycle in the sol-gel process. A similar effect has also been reported by other authors [13]. Notably, in these TiO_2/AC composites, there is no obvious peak at the position of 24.6°, which is the characteristic peak for the (002) plane of AC. The reason could be attributed to the fact that the main peak of AC at 24.6° might be shielded by the peak of anatase TiO_2 at 25.3°. Additionally, the crystal size of TiO_2 in the composite photocatalysts is calculated using Scherrer's equation for the diffraction peak at 25.3° (101 plane) as 12–14 nm.

3.2. TG Analysis. In order to investigate the loading amount of TiO_2 in the TiO_2/AC composites synthesized at different loading cycles, thermogravimetric (TG) tests were carried out in a range of 20–800°C with an air flow. As shown in the TG curves (Figure 2), the gentle weight loss of TiO_2/AC composite at temperatures ranging from 20 to 90°C is generally attributed to the escape of adsorbed water while the obvious weight loss at temperatures from 450 to 550°C is mainly due to the carbons burning off in air. The mass which almost

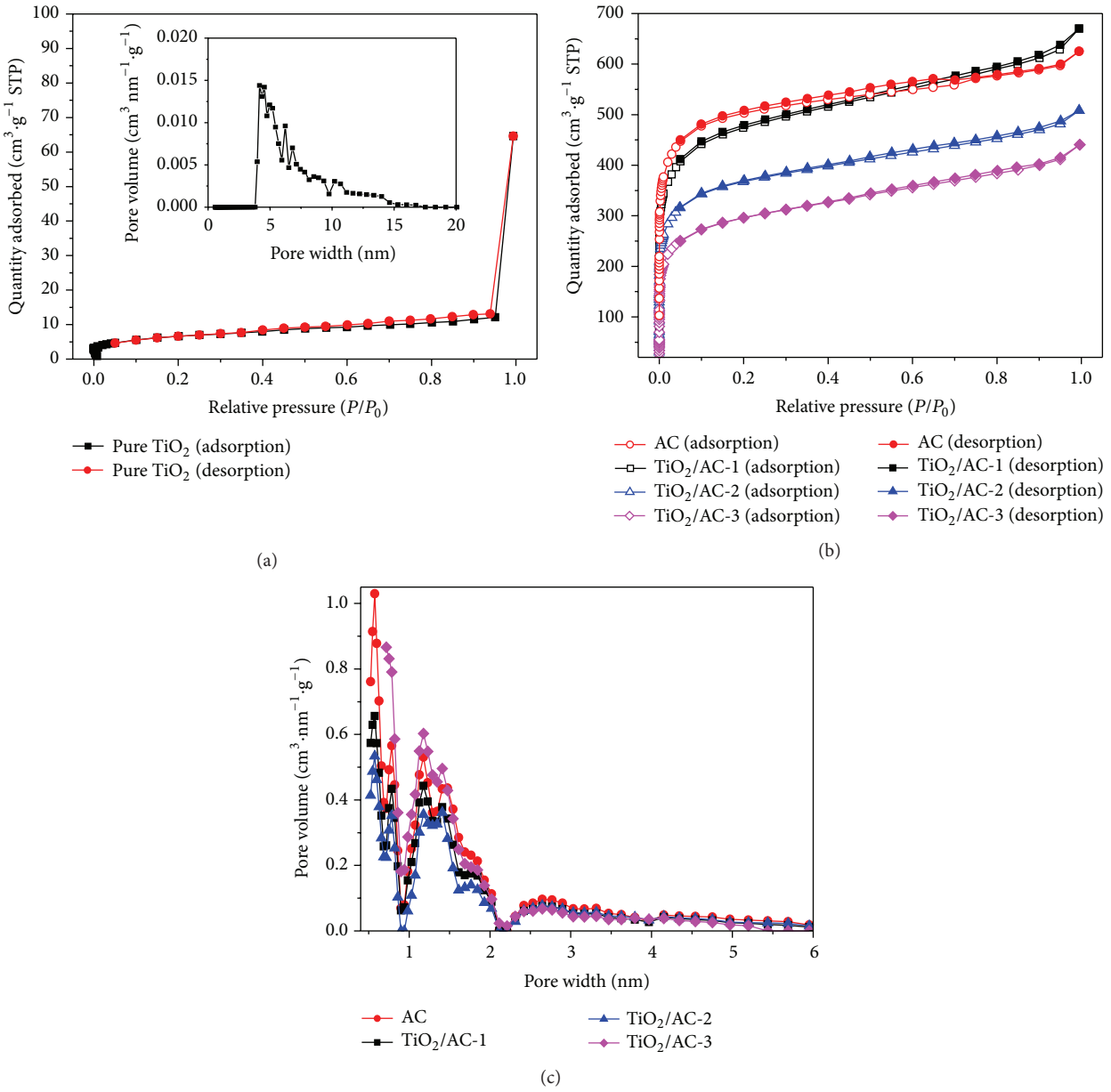

Figure 3: Nitrogen adsorption-desorption isotherms and pore size distributions of pure TiO_2, AC, and TiO_2/AC composites: (a) nitrogen adsorption-desorption isotherm and pore size distribution (inset) of pure TiO_2, (b) nitrogen adsorption-desorption isotherms of AC and TiO_2/AC composites, and (c) pore size distributions of AC and TiO_2/AC composites.

keeps constant in the TG curves after 600°C contains the loaded TiO_2 and ash in AC. According to the TG curves, the weight loss of the three composite photocatalysts decreases with the loading cycle increasing, and the final ash content is about 5.6% for TiO_2/AC-1, 15.8% for TiO_2/AC-2, and 26.9% for TiO_2/AC-3. Hence, the loading amount of TiO_2in the composite photocatalysts synthesized at 1, 2, and 3 loading cycles subtracting the ash content of substrate AC (0.3%) is about 5.3%, 15.5%, and 26.7%, respectively. This result further indicates that the loading cycle has an important influence on the loading amount of TiO_2 in the composite photocatalysts, since more loading cycles lead to more TiO_2 being deposited on the substrate AC surface.

3.3. Pore Structure of TiO_2/AC Composites. The nitrogen adsorption-desorption isotherms and pore size distributions of pure TiO_2, original AC, and the TiO_2/AC composites are presented in Figure 3. For pure TiO_2, a typical type II isotherm (Figure 3(a)) with a small hysteresis phenomenon attributed to aggregation of nanoparticles can be noticed, and this isotherm corresponds to a relatively low porosity material in agreement with the low specific surface area (10 m^2/g) and the negligible micropore volume listed in Table 1. However, the isotherms of AC and TiO_2/AC composites (Figure 3(b)) exhibit a marked increment at the relative pressure of P/P_0 less than 0.1, followed by approximate plateaus at the relative pressure of P/P_0 more than 0.2, indicating that the AC and

Table 1: The specific surface area and pore structure parameters of TiO_2, AC, and TiO_2/AC composites.

Sample	$S_{BET}/(m^2 \cdot g^{-1})$	$S_{mic}/(m^2 \cdot g^{-1})$	$S_{mes}/(m^2 \cdot g^{-1})$	$V_t/(cm^3 \cdot g^{-1})$	$V_{mic}/(cm^3 \cdot g^{-1})$	$V_{mes}/(cm^3 \cdot g^{-1})$
Pure TiO_2	10	0	10	0.057	0	0.057
AC	1576	1298	278	0.967	0.662	0.305
TiO_2/AC-1	1507	1061	446	1.037	0.542	0.495
TiO_2/AC-2	1167	836	331	0.786	0.427	0.359
TiO_2/AC-3	949	616	333	0.682	0.315	0.367

S_{BET}, BET specific surface area; S_{mic}, micropore specific surface; S_{mes}, mesopore specific surface; V_t, total pore volume; V_{mic}, micropore volume; and V_{mes}, mesopore volume.

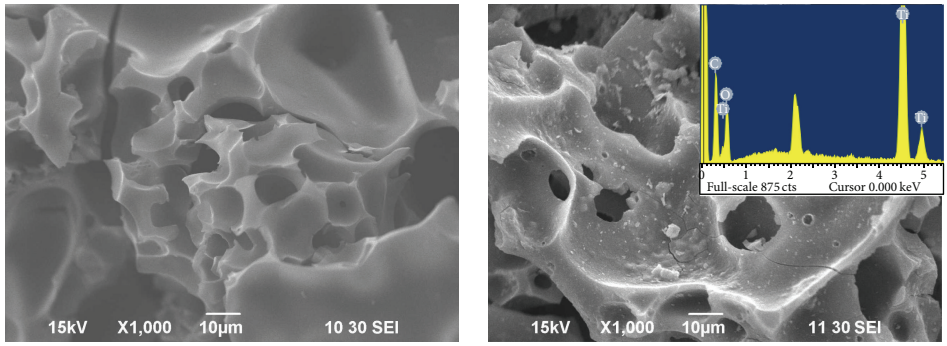

(a) (b)

Figure 4: SEM images of AC and TiO_2/AC-2: (a) AC, (b) TiO_2/AC-2 (inset: EDX spectrum).

the TiO_2/AC composites are essentially microporous materials. Also, the desorption hysteresis loops at a relative pressure of around 0.5 are observed in the isotherms of AC and the TiO_2/AC composites, suggesting the presence of a certain amount of mesopores. From the curves of the DFT pore size distributions of AC and TiO_2/AC composites (Figure 3(c)), it can be seen that the pores of AC and TiO_2/AC composites are distributed in the range of 0.5–6 nm, and the mesopores are mainly distributed between 2.2 nm and 5.0 nm. Furthermore, compared to the original AC, the micropores of TiO_2/AC composites decrease gradually with the increasing of loading cycle, especially for the pore distributed in the range of 0.5–1 nm. The reason can be attributed to the fact that more loading cycles lead to more TiO_2particles being deposited, blocking some micropores of the AC substrate. The specific surface area (S_{BET}), micropore specific surface (S_{mic}), mesopore specific surface (S_{mes}), total pore volume (V_t), micropore volume (V_{mic}), and mesopore specific surface (V_{mes}) of AC are 1576 m^2/g, 1298 m^2/g, 278 m^2/g, 0.967 cm^3/g, 0.662 cm^3/g, and 0.305 cm^3/g (Table 1), respectively. For the TiO_2/AC composites, S_{BET}, S_{mic}, V_t, and V_{mic} decrease gradually with increasing the loading cycles, except that the V_t of TiO_2/AC-1 increases slightly. The increment of V_t of TiO_2/AC-1 is mainly caused by the covering of TiO_2 on the AC surface and forms a small number of mesopores in the composite photocatalyst to increase the pore volume. In addition, it is worthy of noting that S_{mic} and V_{mic} of composite photocatalyst decrease from 1298 m^2/g and 0.662 cm^3/g to 616 m^2/g and 0.315 cm^3/g when the original AC was loaded by TiO_2 3 times, whereas its S_{mes} and V_{mes} present a slight increment. The results further confirm that some micropores are blocked or covered by the TiO_2 particles.

3.4. SEM and TEM Analysis. The morphologies of the original AC and the TiO_2/AC-2 composite photocatalyst were investigated by SEM micrographs. As shown in Figure 4, the original AC displays a uniform morphology with irregular and highly porous surface, indicating well-developed porosity (Figure 4(a)). The surface of the TiO_2/AC-2 is homogeneously covered with TiO_2 particles without apparent agglomeration in local area (Figure 4(b)). Also, the TiO_2 particles deposit not only on the surface but also on the mesopores and macrospores of AC, which will increase the probability of receiving light and exhibiting higher photocatalytic activity [13]. In addition, the energy dispersive X-ray (EDX) spectrum of TiO_2/AC-2 (Figure 4(b), inset) shows that the presence of C, Ti, and O is the main element for the composite, suggesting that the TiO_2/AC composites with high purity have been successfully synthesized in this study.

Further evidence was provided by the TEM micrographs shown in Figure 5. It is clearly indicated that the TiO_2 particle (black region) with nanosized dimension is uniformly deposited on the surface as well as in the bulk of the AC (gray region), and the large scale agglomerate is not detected in the TiO_2/AC composites synthesized at 1 and 2 loading cycles (Figures 5(a) and 5(b)). However, when the TiO_2/AC-3 photocatalyst was synthesized at 3 loading cycles, the as-formed TiO_2particles are inclined to agglomerate (Figure 5(c)). It suggests that the TiO_2particles are easier to agglomerate on the surface of the TiO_2/AC composites with increasing

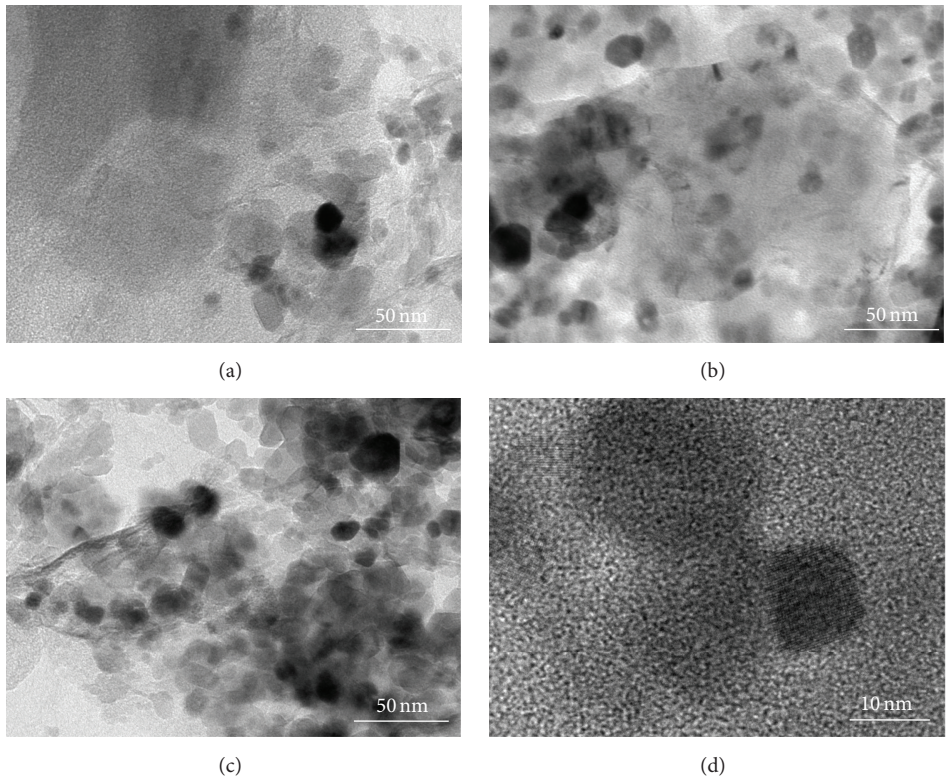

Figure 5: TEM micrographs of TiO_2/AC composites: (a) TiO_2/AC-1, (b) TiO_2/AC-2, (c) TiO_2/AC-3, and (d) HRTEM image of TiO_2/AC-2.

the loading cycle. It is well known that the photocatalytic activity of TiO_2 composite functional materials strongly depends on their morphological structure [14, 38]. Compared with the TiO_2 particles deposited homogeneously on the surface of TiO_2/AC-1 and TiO_2/AC-2, the agglomerated TiO_2 particles in the TiO_2/AC-3 composites may hamper the light incidence on these photoreactive sites and consequently reduce its photocatalytic degradation efficiency. Furthermore, the TiO_2 particle size in composite photocatalyst can be estimated to about 10–20 nm in the high resolution TEM image (Figure 5(d)), which is good in accordance with the crystal size obtained by means of XRD pattern.

3.5. Photocatalytic Degradation of RhB. Photocatalytic activity for the obtained pure TiO_2 as well as TiO_2/AC composites was estimated by measuring the decomposition rate of RhB in aqueous solution in the presence of UV light irradiation, and the results are shown in Figure 6. For the original AC (Figure 6(a)), the removal of RhB increases gradually with the increasing adsorption time, and about 71.0% of the initial RhB is removed until reaching the adsorption equilibrium at the end of 90 min in the dark. The removal rate of RhB is almost unchanged with increasing the adsorption time in the UV light irradiation. Nevertheless, the RhB removal rate of pure TiO_2 is negligible when the solution is kept in the dark for 90 min but increases noticeably with prolonging the time of UV light irradiation, and the final removal rate of RhB reaches only 55.8%, which is mainly attributed to the photocatalytic degradation process. However, for the TiO_2/AC composites (Figure 6(b)), the RhB removal process in aqueous solution can be divided into two stages: the removal process of 90 min in the dark, which is mainly attributed to the adsorption effect of TiO_2/AC composites. The other stage is the 120 min in the UV light irradiation, which is mainly caused by the photocatalytic degradation. In this paper, the concentration of RhB maintained in the aqueous solution at the end of adsorption stage in the dark is taken as the starting concentration of RhB in the photocatalytic degradation stage, and the degradation percentages of TiO_2/AC composites were calculated according to this reference. As shown in Figure 6, the initial removal rate of TiO_2/AC composites was similar to AC, but, after 90 min in the dark, the TiO_2/AC composites are still able to remove the RhB by the photocatalytic degradation effect on the UV light irradiation; as a result, the percentages of RhB removal continue to increase. The final percentages of RhB removed by TiO_2/AC-1, TiO_2/AC-2, and TiO_2/AC-3 reach 82.0%, 93.2%, and 86.3%, respectively. The RhB removal rate of TiO_2/AC composites is far superior for pure TiO_2 synthesized in this study or macroporous TiO_2 photocatalyst reported in our previous work [39].

Based on the results that the percentages of RhB removal are 66.1%, 46.7%, and 38.9% after 90 min in the dark by adsorption, the photocatalytic degradation percentage of RhB is 15.9% for TiO_2/AC-1, 46.5% for TiO_2/AC-2, and 47.4% for TiO_2/AC-3, respectively. Clearly, the photocatalytic degradation percentage of RhB for TiO_2/AC-2 is almost

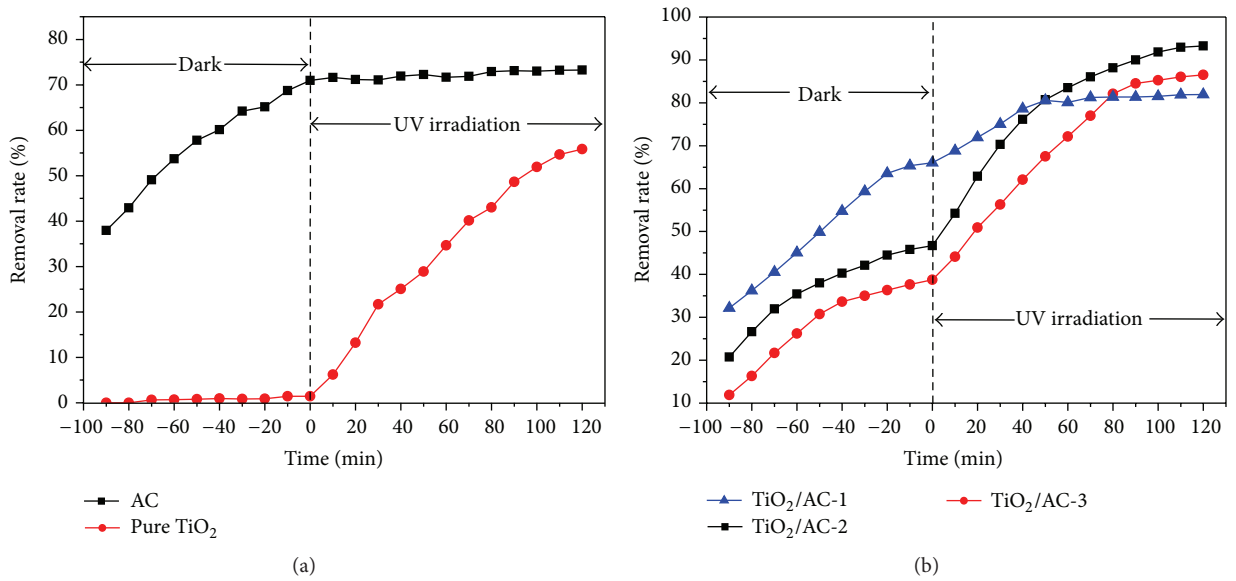

Figure 6: RhB removal rate of pure TiO_2, AC, and composite photocatalysts: (a) pure TiO_2 and AC, (b) TiO_2/AC composite photocatalysts.

equivalent to that for TiO_2/AC-3, but the loading amount of TiO_2 in TiO_2/AC-2 for 15.5% is lower than that in TiO_2/AC-3 for 26.7%, indicating that the photocatalytic activity of nanosized TiO_2 in TiO_2/AC-2 is higher than that in TiO_2/AC-3. The fundamental mechanism for this can be clarified as follows: the TiO_2/AC composites exhibit the dual functions such as absorption and photocatalytic degradation to remove the RhB in the aqueous solution [13, 38, 40]; the proposed schematic illustration is shown in Figure 7, which is also similar to the case on the photocatalyst of TiO_2/ACF nanocomposites [41]. Under dark condition, the removal process depends strongly on the adsorption performance of substrate AC. However, under UV light irradiation, the RhB removal process requires the pollutant to be adsorbed on the TiO_2/AC composites surface prior to immediate photocatalytic degradation [15, 42]. Therefore, the efficiency of photocatalytic reaction can be affected by the adsorption performance of substrate AC and the photocatalytic activity nanosized TiO_2 particles.

For the TiO_2/AC-1, the RhB removed by adsorption is predominant because of its well-developed porosity, and the final RhB removal rate reaches 82.0%, while the photocatalytic degradation percentage of RhB is only 15.9%, which may be ascribed to the limited TiO_2 particles that deposited on the composite photocatalyst. With the increasing loading cycle during the preparation of TiO_2/AC composites, more TiO_2will be exposed on the surface of AC. As a result, photoreactive sites available on the AC surface increase, which contributes to the high photocatalytic activity of TiO_2/AC composites. Therefore, the photocatalytic degradation percentage of RhB for TiO_2/AC-2 can reach 46.5%, and the final RhB removal rate can reach 93.2% even if the adsorption effect is weakened due to the reduced porosity of composite photocatalyst. However, for the TiO_2/AC-3, the photocatalytic degradation percentage of RhB is not enhanced as expected in terms of the loading amount of TiO_2 in composite photocatalyst. The reason may be attributed to the fact that a certain amount of nanosized TiO_2 particles aggregates on the surface of TiO_2/AC-3, which can reduce the efficient UV light absorption and decrease the photoreactive sites for degradation. On the other hand, the reduction of the porosity results in the fact that the RhB adsorbed on the TiO_2/AC composites surface is very limited, and the efficiency of photocatalytic degradation is also restricted consequently. The results indicate clearly that the morphological structure of TiO_2/AC composites such as porosity and the dispersibility of TiO_2 particles on the surface of composite photocatalyst are crucial for obtaining high photocatalytic activity. Therefore, the loading cycle is considered a significant factor in preparation of TiO_2/AC composites by sol-gel method.

4. Conclusions

It is found that TiO_2/AC composites can be synthesized simply by sol-gel method under calcination at 500°C. The TiO_2 particles deposited on the AC surface display mainly anatase crystal structure with a crystallite size of 10–20 nm. The morphological structure and photocatalytic activity of composite photocatalyst are strongly dependent on the loading cycle. The porosity of TiO_2/AC composites may decrease gradually and the dispersibility of TiO_2 particles on the AC surface becomes less uniform after multiloading cycles due to more TiO_2 particles deposited on the AC surface, which leads to blocking or covering of part of the micropores. The photocatalytic degradation of RhB experiments indicates that the optimized composite photocatalyst of TiO_2/AC-2 synthesized at 2 loading cycles demonstrates the highest photocatalytic activity, which can lead to 93.2% RhB being rapidly removed from aqueous solution under UV light irradiation. The high removal rate of RhB of TiO_2/AC composite is attributed to the excellent adsorption effect in the dark and

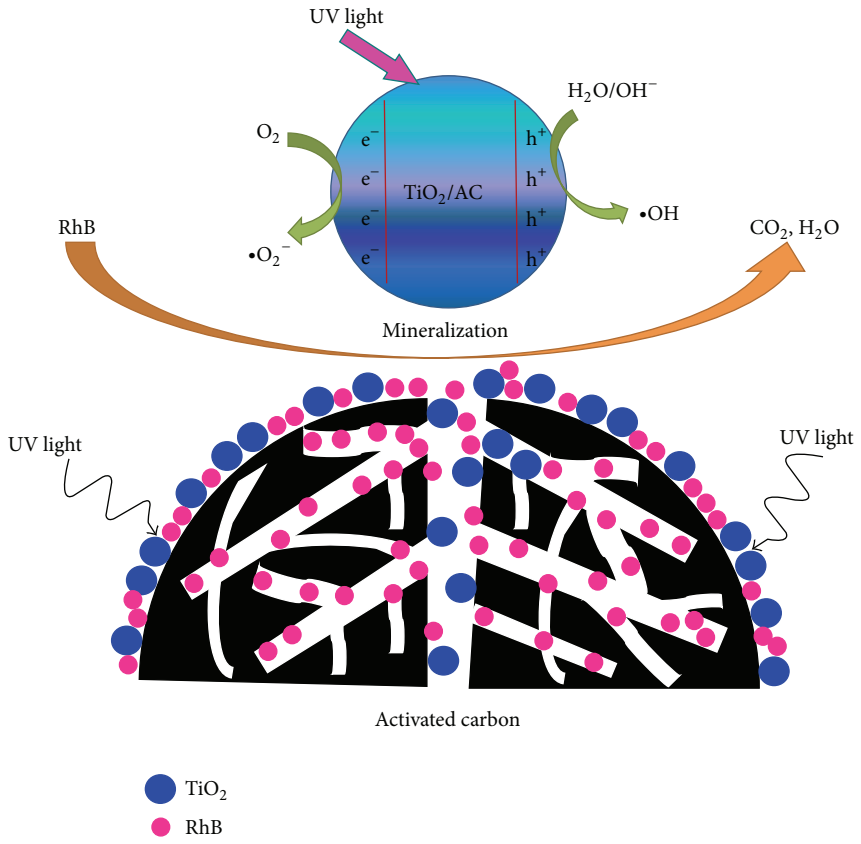

Figure 7: Proposed schematic illustration for the adsorption and photocatalytic degradation of RhB on the TiO_2/AC composites under UV light irradiation.

high efficiency photocatalytic degradation in the presence of UV light irradiation.

Conflict of Interests

The authors declare that there is no conflict of interests regarding the publication of this paper.

Acknowledgments

The authors gratefully acknowledge the financial support of the National Natural Science Foundation of China (51404098, 51174077, 51404097, and U1361119), International Science and Technology Cooperation Project of Henan province (152102410047), Education Department Science Foundation of Henan province (13A430336), and Opening Project of Henan Key Discipline Open Laboratory of Mining Engineering Materials (MEM13-7, MEM13-12, and MEM14-5).

References

[1] M. Rafatullah, O. Sulaiman, R. Hashim, and A. Ahmad, "Adsorption of methylene blue on low-cost adsorbents: a review," *Journal of Hazardous Materials*, vol. 177, no. 1–3, pp. 70–80, 2010.

[2] V. K. Gupta, R. Kumar, A. Nayak, T. A. Saleh, and M. A. Barakat, "Adsorptive removal of dyes from aqueous solution onto carbon nanotubes: a review," *Advances in Colloid and Interface Science*, vol. 193-194, pp. 24–34, 2013.

[3] N. M. Mahmoodi, R. Salehi, M. Arami, and H. Bahrami, "Dye removal from colored textile wastewater using chitosan in binary systems," *Desalination*, vol. 267, no. 1, pp. 64–72, 2011.

[4] N. F. Cardoso, E. C. Lima, B. Royer et al., "Comparison of *Spirulina platensis* microalgae and commercial activated carbon as adsorbents for the removal of Reactive Red 120 dye from aqueous effluents," *Journal of Hazardous Materials*, vol. 241-242, pp. 146–153, 2012.

[5] M. Asiltürk and Ş. Şener, "TiO_2-activated carbon photocatalysts: preparation, characterization and photocatalytic activities," *Chemical Engineering Journal*, vol. 180, pp. 354–363, 2012.

[6] Z. H. Zhang, Y. Xua, X. P. Ma et al., "Microwave degradation of methyl orange dye in aqueous solution in the presence of nano-TiO_2-supported activated carbon (supported-TiO_2/AC/MW)," *Journal of Hazardous Materials*, vol. 209–210, pp. 271–277, 2012.

[7] V. K. Gupta and Suhas, "Application of low-cost adsorbents for dye removal—a review," *Journal of Environmental Management*, vol. 90, no. 8, pp. 2313–2342, 2009.

[8] Y. J. Li, X. M. Zhou, W. Chen et al., "Photodecolorization of Rhodamine B on tungsten-doped TiO_2/activated carbon under visible-light irradiation," *Journal of Hazardous Materials*, vol. 227-228, pp. 25–33, 2012.

[9] P. Jiang, D. Ren, D. He, W. Fu, J. Wang, and M. Gu, "An easily sedimentable and effective TiO_2 photocatalyst for removal of

dyes in water," *Separation and Purification Technology*, vol. 122, pp. 128–132, 2014.

[10] E. Forgacs, T. Cserháti, and G. Oros, "Removal of synthetic dyes from wastewaters: a review," *Environment International*, vol. 30, no. 7, pp. 953–971, 2004.

[11] M. H. Do, N. H. Phan, T. D. Nguyen et al., "Activated carbon/Fe_3O_4 nanoparticle composite: fabrication, methyl orange removal and regeneration by hydrogen peroxide," *Chemosphere*, vol. 85, no. 8, pp. 1269–1276, 2011.

[12] P.-J. Lu, H.-C. Lin, W.-T. Yu, and J.-M. Chern, "Chemical regeneration of activated carbon used for dye adsorption," *Journal of the Taiwan Institute of Chemical Engineers*, vol. 42, no. 2, pp. 305–311, 2011.

[13] G. Xue, H. H. Liu, Q. Y. Chen, C. Hills, M. Tyrer, and F. Innocent, "Synergy between surface adsorption and photocatalysis during degradation of humic acid on TiO_2/activated carbon composites," *Journal of Hazardous Materials*, vol. 186, no. 1, pp. 765–772, 2011.

[14] Y.-J. Xu, Y. B. Zhuang, and X. Z. Fu, "New insight for enhanced photocatalytic activity of TiO_2 by doping carbon nanotubes: a case study on degradation of benzene and methyl orange," *Journal of Physical Chemistry C*, vol. 114, no. 6, pp. 2669–2676, 2010.

[15] T.-T. Lim, P.-S. Yap, M. Srinivasan, and A. G. Fane, "TiO_2/AC composites for synergistic adsorption-photocatalysis processes: present challenges and further developments for water treatment and reclamation," *Critical Reviews in Environmental Science and Technology*, vol. 41, no. 13, pp. 1173–1230, 2011.

[16] C. Andriantsiferana, E. F. Mohamed, and H. Delmas, "Photocatalytic degradation of an azo-dye on TiO_2/activated carbon composite material," *Environmental Technology*, vol. 35, no. 3, pp. 355–363, 2014.

[17] A. E. Eliyas, L. Ljutzkanov, I. D. Stambolova et al., "Visible light photocatalytic activity of TiO_2 deposited on activated carbon," *Central European Journal of Chemistry*, vol. 11, no. 3, pp. 464–470, 2013.

[18] W. Y. Dong, C. W. Lee, X. C. Lu et al., "Synchronous role of coupled adsorption and photocatalytic oxidation on ordered mesoporous anatase TiO_2–SiO_2 nanocomposites generating excellent degradation activity of RhB dye," *Applied Catalysis B: Environmental*, vol. 95, no. 3-4, pp. 197–207, 2010.

[19] X. D. Wang, F. Shi, W. Huang, and C. M. Fan, "Synthesis of high quality TiO_2 membranes on alumina supports and their photocatalytic activity," *Thin Solid Films*, vol. 520, no. 7, pp. 2488–2492, 2012.

[20] S. K. Padmanabhan, S. Pal, E. Ul Haq, and A. Licciulli, "Nanocrystalline TiO_2-diatomite composite catalysts: effect of crystallization on the photocatalytic degradation of rhodamine B," *Applied Catalysis A: General*, vol. 485, pp. 157–162, 2014.

[21] M. N. Chong, Z. Y. Tneu, P. E. Poh, B. Jin, and R. Aryal, "Synthesis, characterisation and application of TiO_2-zeolite nanocomposites for the advanced treatment of industrial dye wastewater," *Journal of the Taiwan Institute of Chemical Engineers*, vol. 50, pp. 288–296, 2015.

[22] V. Belessi, D. Lambropoulou, I. Konstantinou et al., "Structure and photocatalytic performance of TiO_2/clay nanocomposites for the degradation of dimethachlor," *Applied Catalysis B: Environmental*, vol. 73, no. 3, pp. 292–299, 2007.

[23] E. Rossetto, D. I. Petkowicz, J. H. Z. dos Santos, S. B. C. Pergher, and F. G. Penha, "Bentonites impregnated with TiO_2 for photodegradation of methylene blue," *Applied Clay Science*, vol. 48, no. 4, pp. 602–606, 2010.

[24] M. S. A. S. Shah, A. R. Park, K. Zhang, J. H. Park, and P. J. Yoo, "Green synthesis of biphasic TiO_2-reduced graphene oxide nanocomposites with highly enhanced photocatalytic activity," *ACS Applied Materials and Interfaces*, vol. 4, no. 8, pp. 3893–3901, 2012.

[25] L. Zhu, S. B. Jo, J. H. Jo, S. Ye, K. Ullah, and W. C. Oh, "Characterization of a novel MnS-ACF/TiO_2 composite and photocatalytic mechanism derived from organic dye decomposition," *Journal of the Korean Ceramic Society*, vol. 51, no. 3, pp. 139–144, 2014.

[26] W. J. Lee, J. M. Lee, S. T. Kochuveedu et al., "Biomineralized N-doped CNT/TiO_2 core/shell nanowires for visible light photocatalysis," *ACS Nano*, vol. 6, no. 1, pp. 935–943, 2012.

[27] P. Muthirulan, C. K. Nirmala Devi, and M. Meenakshi Sundaram, "Fabrication and characterization of efficient hybrid photocatalysts based on titania and graphene for acid orange seven dye degradation under UV irradiation," *Advanced Materials Letters*, vol. 5, no. 4, pp. 163–171, 2014.

[28] H. Slimen, A. Houas, and J. P. Nogier, "Elaboration of stable anatase TiO_2 through activated carbon addition with high photocatalytic activity under visible light," *Journal of Photochemistry and Photobiology A: Chemistry*, vol. 221, no. 1, pp. 13–21, 2011.

[29] X. J. Wang, Y. F. Liu, Z. H. Hu, Y. J. Chen, W. Liu, and G. H. Zhao, "Degradation of methyl orange by composite photocatalysts nano-TiO_2 immobilized on activated carbons of different porosities," *Journal of Hazardous Materials*, vol. 169, no. 1–3, pp. 1061–1067, 2009.

[30] T. S. Jamil, M. Y. Ghaly, N. A. Fathy, T. A. Abd El-Halim, and L. Österlund, "Enhancement of TiO_2 behavior on photocatalytic oxidation of MO dye using TiO_2/AC under visible irradiation and sunlight radiation," *Separation and Purification Technology*, vol. 98, pp. 270–279, 2012.

[31] Z. He, S. Yang, Y. Ju, and C. Sun, "Microwave photocatalytic degradation of Rhodamine B using TiO_2 supported on activated carbon: mechanism implication," *Journal of Environmental Sciences*, vol. 21, no. 2, pp. 268–272, 2009.

[32] Y. H. Zhang, Z. R. Tang, X. Z. Fu, and Y. J. Xu, "TiO_2-graphene nanocomposites for gas-phase photocatalytic degradation of volatile aromatic pollutant: is TiO_2-graphene truly different from other TiO_2-carbon composite materials?" *ACS Nano*, vol. 4, no. 12, pp. 7303–7314, 2010.

[33] J. R. Utrilla, M. S. Polo, M. M. Abdeldaiem, and R. O. Pérez, "Role of activated carbon in the photocatalytic degradation of 2,4-dichlorophenoxyacetic acid by the UV/TiO_2/activated carbon system," *Applied Catalysis B: Environmental*, vol. 126, pp. 100–107, 2012.

[34] C. Zhang, D. Long, B. Xing et al., "The superior electrochemical performance of oxygen-rich activated carbons prepared from bituminous coal," *Electrochemistry Communications*, vol. 10, no. 11, pp. 1809–1811, 2008.

[35] H. P. Klug and L. E. Alexander, *X-Ray Diffraction Procedures for Polycrystalline and Amorphous Materials*, John Wiley & Sons, New York, NY, USA, 2nd edition, 1974.

[36] Z. L. Zhu, A. M. Li, S. Zhong, F. Q. Liu, and Q. X. Zhang, "Preparation and characterization of polymer-based spherical activated carbons with tailored pore structure," *Journal of Applied Polymer Science*, vol. 109, no. 3, pp. 1692–1698, 2008.

[37] D. Huang, Y. Miyamoto, T. Matsumoto et al., "Preparation and characterization of high-surface-area TiO_2/activated carbon by low-temperature impregnation," *Separation and Purification Technology*, vol. 78, no. 1, pp. 9–15, 2011.

[38] S. G. Kumar and L. G. Devi, "Review on modified TiO_2 photocatalysis under UV/visible light: selected results and related mechanisms on interfacial charge carrier transfer dynamics," *Journal of Physical Chemistry A*, vol. 115, no. 46, pp. 13211–13241, 2011.

[39] G. Yi, B. Xing, J. Jia et al., "Fabrication and characteristics of macroporous TiO_2 photocatalyst," *International Journal of Photoenergy*, vol. 2014, Article ID 783531, 7 pages, 2014.

[40] C. K. Gu and C. Shannon, "Investigation of the photocatalytic activity of TiO_2–polyoxometalate systems for the oxidation of methanol," *Journal of Molecular Catalysis A: Chemical*, vol. 262, no. 1-2, pp. 185–189, 2007.

[41] X. D. Wang, K. Zhang, X. L. Guo, G. D. Shen, and J. Y. Xiang, "Synthesis and characterization of N-doped TiO_2 loaded onto activated carbon fiber with enhanced visible-light photocatalytic activity," *New Journal of Chemistry*, vol. 38, no. 12, pp. 6139–6146, 2014.

[42] A. Omri and M. Benzina, "Almond shell activated carbon: adsorbent and catalytic support in the phenol degradation," *Environmental Monitoring and Assessment*, vol. 186, no. 6, pp. 3875–3890, 2014.